Frontiers of Information Technology & Electronic Engineering
www.zju.edu.cn/jzus; engineering.cae.cn; www.springerlink.com
ISSN 2095-9184 (print); ISSN 2095-9230 (online)
E-mail: jzus@zju.edu.cn

New technique:

Flexible resonant tank for a combined converter to achieve an HPS and LED compatible driver*

Jin HU†, Hui-pin LIN†, Zheng-yu LU†‡, Feng-wu ZHOU
(*College of Electrical Engineering, Zhejiang University, Hangzhou 310027, China*)
†E-mail: justinhu2008@hotmail.com; linhuipin@126.com; eeluzy@zju.edu.cn

Received Feb. 10, 2015; Revision accepted May 30, 2015; Crosschecked July 14, 2015

Abstract: High pressure sodium (HPS) lamp has been widely used in street lighting applications because of its maturity, reliability, high lighting efficiency, long life-time, and low cost. Light emitting diode (LED) is expected as the next generation lighting source due to its continuously improving luminous efficacy, better color characteristic, and super long life-time. The two lighting sources may coexist in street lighting applications for a long time. A novel HPS and LED compatible driver is proposed which is rather suitable and flexible for driving HPS and LED in street lighting applications. The proposed driver combines the LLC and LCC resonant circuits into a flexible resonant tank. The flexible resonant tank may change to LLC or isolated LCC circuit according to the lighting source. It inherits the traditional HPS and LED drivers' zero voltage switching (ZVS) characteristics and dimmable function. The design of the proposed flexible resonant tank considers the requirements of both HPS and LED. The experiments of driving HPS and LED on a prototype driver show that the driver can drive the two lighting sources flexibly with high efficiency.

Key words: High pressure sodium (HPS), Light emitting diode (LED), Compatible driver, Ballast
doi:10.1631/FITEE.1500054 **Document code:** A **CLC number:** TM923.61

1 Introduction

High pressure sodium (HPS) lamp has advantageous characteristics such as high lighting efficiency, long life-time, and low cost (IEC, 2011). It has been used all over the world as the street lighting source for several decades, which proves its maturity and reliability in outdoor lighting applications.

Thanks to the advantages in terms of luminous efficacy, color characteristic, and life-time, light emitting diode (LED) is expected as the next generation lighting source (Azevedo *et al*., 2009; Tan, 2010). Its luminous efficacy has been improved and the cost reduced in the past years.

However, till now, the cost, reliability, and lighting efficiency of LED have no clear advantage over HPS. HPS is still preferred in most street lighting applications, especially for streets in the downtown. By using new craftwork, ballast, and remote control technologies, there may be further improvements in terms of energy saving, life time increase, and cost reduction of HPS solutions (Wei *et al*., 2009; Tomoroga *et al*., 2012; Zotos *et al*., 2012; Kirsten *et al*., 2013; Schnell *et al*., 2013). Generally, it needs time for new technologies such as LED to be widely accepted. There is a great possibility that both HPS and LED will be used as street lighting sources for a long time.

In a typical street lighting system, HPS and LED may both be used. As shown in Fig. 1, the conventional road lighting solution needs many kinds of ballasts and drivers to drive different types of lighting sources. For most manufactures, they need to deal with many types of ballasts. This requires a large amount of investment and a high level of production

‡ Corresponding author
* Project supported by the National Natural Science Foundation of China (No. 51177148)
ORCID: Jin HU, http://orcid.org/0000-0001-7833-7138

Fig. 1 HPS, LED and their compatible driving solutions for a typical road lighting application

management ability. For users, different types of ballasts make the installing and repairing not so convenient because people have to learn about a lot of different applications. In consumer electronics applications, multi-functional products, such as mobile phone, charger (Choi *et al*., 2013), and ballast (Cheong *et al*., 2006; Lee and Hui, 2009), have been accepted by the market. In industrial applications, multi-functional power supplies, such as uninterruptible power supply (UPS) and inverters reported in the literature (Ko *et al*., 2007; Zhao *et al*., 2013), also accommodate different applications, which bring facility for the users. Therefore, if the HPS ballast and LED driver can be designed to be compatible and universal, it will be a candidate for some producers and users. This multi-functional driving solution can save resources for the society, cut down the research and development investments for the producers, and make the implementation simpler for the users.

However, the driving methods of HPS and LED are different. HPS lamp should be driven in AC constant power mode like the applications in Huang *et al*. (2007) and Cheng *et al*. (2014), while LED should be driven in DC constant current (CC) mode like the applications in Mu *et al*. (2011), Wang H *et al*. (2011),and Wu *et al*. (2011). The output voltage of the LED driver should be limited to the constant voltage (CV) mode in the light load or open circuit condition. The most popular LED drivers for street lighting usually use isolated topologies, which are helpful for satisfying the safety requirements (IEC, 2006). According to the different driving methods, the topologies of the drivers are different. The LCC resonant converter is one of the popular solutions to HPS ballast (Cardesin *et al*., 2005; Rodrigues *et al*., 2009; Zhu *et al*., 2009; Wu *et al*., 2011) due to its high efficiency and large range of gain, while the LLC resonant converter has been widely used for the LED driver due to its soft-switching and isolation characteristics (Chen *et al*., 2011; Chang *et al*., 2012; Shrivastava and Singh, 2012).

The design methods for the two circuits are also different and incompatible. For the LCC converter, the design usually needs to consider the different gains of the resonant tank in HPS ignition, run-up, and burn stages. Traditional design of the LLC

converter in LED applications cares about the maximum output current and dimming conditions (Chen *et al*., 2011).

Some efforts have been made in research on compatible driving technologies for different lighting sources. Nan and Chung (2011) considered the tube fluorescent lamp and tube LED application in indoor applications and tried a way to make these two different lighting sources compatible, wherein LED can be connected to ballast's output directly. It avoids resource waste when a tube LED is used to replace a tube fluorescent lamp. In Visconti *et al*. (2011), the ballast drove high intensity discharge (HID) lamp or LED by the choice of a controllable switch. In the LED driving mode, the LED is connected to the HID ballast by a rectifier but without magnetic isolation. Non-isolation in the LED driving mode is not helpful for safety consideration in street lighting applications. Costantini *et al*. (2011) proposed a CMOS low-power system-on-chip (SoC) as a key control circuit of an HID and LED lamp compatible ballast. A low-frequency square waveform is generated to drive HID or LED both without isolation. LED load is proposed to be made up by one or more pairs of anti-parallel connected LED strings. However, this solution seems not efficient because only half of LEDs work at the same time.

In this paper we propose a multi-functional driver which can drive HPS or LED compatibly. Because the structures of the LCC and LLC converters are similar, it is possible to multiplex the resonant components and control circuits to save the cost and reduce the size. Based on comparison between the popular LCC for HPS and LLC for LED, a variable resonant tank is proposed, which can drive these two lighting sources universally. It works as an equivalent LLC resonant tank in the LED driving mode or an equivalent LCC resonant tank in the HPS driving mode. The zero voltage switching (ZVS) characteristics of the conventional LLC and LCC are maintained to achieve high efficiency. In addition, the dimming function is kept for street lighting applications. When the resonant tank is switched to LLC, another advantage is that the tolerance of the resonant inductor can be well controlled to a small range for better consistency in mass production. Moreover, the compromise made in this universal driver is analyzed. Compared with the conventional HPS ballast or LED driver, the bill-of-material (BOM) cost and efficiency may be penalized slightly. Nevertheless, the compatibility and universality properties may bring convenience for some applications.

Besides introducing the working principle of the proposed driver, the parameter analysis of the resonant tank is provided based on exploring the transfer function of the resonant tank in the HPS and LED driving modes. The design of the proposed flexible resonant tank considers the requirements of both HPS and LED applications into consideration. This is different from the conventional LLC LED and LCC HPS design methods (Correa *et al*., 2002; Alonso *et al*., 2003; Moksoon *et al*., 2008; Chen *et al*., 2011).

2 Proposed HPS and LED compatible driving technology

In this section, we illustrate the scheme of the driver and introduce how to choose HPS and LED working modes. Then the working processes of HPS and LED working modes are analyzed.

A compatible driver is proposed (Fig. 2), which can compatibly drive HPS and LED. The driver includes two stages. Power factor corrector (PFC) is the first stage to obtain a high power factor (PF) and a stable DC voltage BUS. The second stage is a half-bridge serially connected to the PFC. The resonant tank includes an inductor L_s, a capacitor C_s, a capacitor C_p, and a transformer T. The transformer T has three windings. The transformer's magnetizing inductor is L_m, and the turn ratio of primary winding to secondary windings is N:1:1. For conciseness, the protection circuits, some simple and well-known circuits are not shown here.

The driver has two output ports. One is for LED, and the other for HPS. The LED load is connected to a capacitor C_{out} in parallel, which is coupled to the secondary winding of transformer T through a full-wave rectifier consisting of diodes D_1 and D_2. The HPS is connected to capacitor C_p in parallel. Correspondingly, the driver has HPS and LED driving modes controlled by switches S_1 and S_2.

A voltage controlled oscillator (VCO) circuit in IC L6574 (STMicroelectronics) generates a clock to control M_1 and M_2 by using a well-known sweeping frequency method. An operational amplifier (OPA) circuit offers an error voltage signal as the input voltage of the VCO.

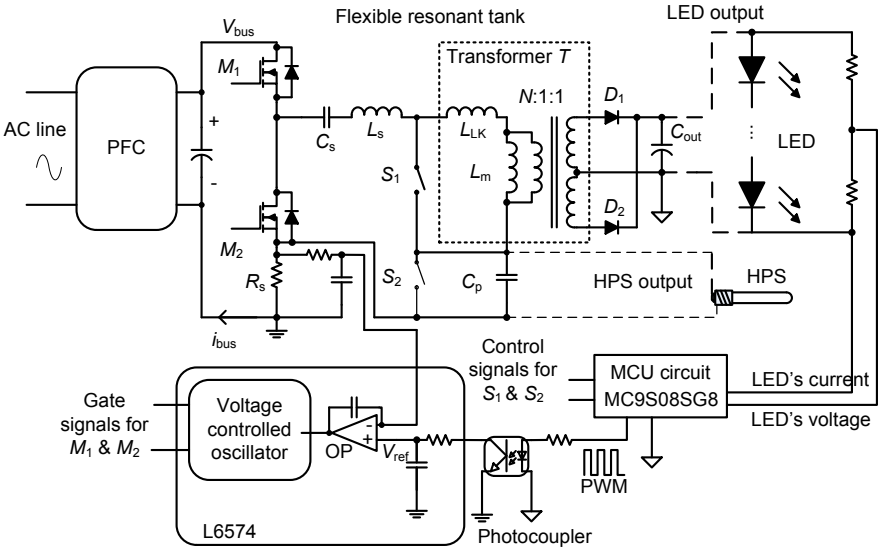

Fig. 2 HPS and LED compatible driver

An MCU MC9S08SG8 (Freescale, USA) is used to choose HPS or LED driving mode. Both the voltage and current of LED are sensed by the MCU. If the current is not zero, the MCU judges that the LED load is connected, and consequently turns S_1 off and S_2 on, to make the driver work in the LED driving mode. It provides a pulse width modulation (PWM) signal, which is transferred through a photocoupler and filtered into a smooth DC reference voltage V_{ref}. V_{ref} is provided to the OPA to regulate the half-bridge's input current, which makes the output LED current constant. If LED current is zero, the driver gets into the HPS driving mode with switch S_1 on and S_2 off. The MCU offers V_{ref} to the OPA to make half-bridge's average input current constant, which makes the power of the half-bridge constant as the input voltage of the half-bridge is stable.

2.1 HPS driving mode

In the HPS driving mode, switch S_1 is turned on and S_2 off. The flexible resonant tank changes to LCC structure (Fig. 3a). The primary winding of transformer T is shorted; therefore, the series inductor L_s functions as a resonant inductor. The converter can work at a high operating frequency (dozens of kHz), which does not lead to the acoustic resonance issue of HPS. This is proven by existing research (Correa *et al.*, 2002; Cardesin *et al.*, 2005; Wang Y *et al.*, 2011).

In this solution, the half-bridge drives the LCC resonant tank. The ZVS of MOSFET is realized to reduce the switching power loss. Even when the output lines are short circuit, ZVS characteristic can still be achieved. It is rather suitable for short circuit protection. The control circuit is based on the IC L6574 and the MCU. The control scheme is as introduced above. The feedback mechanism can be understood by referring to STMicroelectronics AN2708 (STMicroelectronics, 2015a).

The input voltage $V_{in}(t)$ of the resonant tank can be expressed in Fourier series and used hereafter:

$$V_{in}(t)=\frac{V_{bus}}{2}+\frac{2}{\pi}V_{bus}\sum_{n=1,3,5}\frac{1}{n}\sin(n\cdot 2\pi ft). \quad (1)$$

The transfer function of the resonant tank is expressed as

$$G_{HPS}(s)=\frac{1}{L_sC_ps^2+\frac{L_s}{R_H}s+\frac{1}{R_HC_s}s+\frac{C_p}{C_s}+1}. \quad (2)$$

Take driving 150 W HPS as an example. The working process of the half-bridge includes three stages: ignition, run-up, and burn. The gain curves of the resonant tank in different stages are given in Fig. 3b according to Eq. (2).

Stage 1: ignition. The 3rd order harmonic of $V_{in}(t)$ is used to ignite HPS (Alonso *et al.*, 2003). The HPS model is very complicated. For clear and easy analysis, HPS is simplified into an equivalent resistor R_H. Before HPS is ignited, the resistance of R_H can be considered infinitely large.

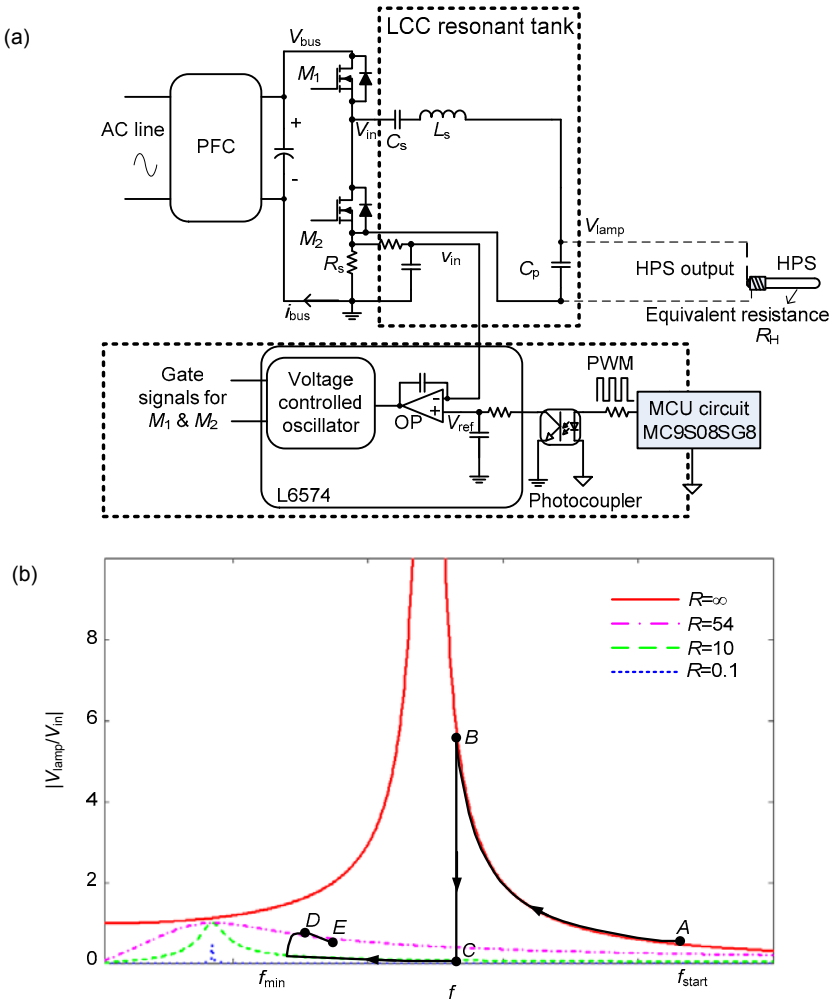

Fig. 3 The driver in the HPS driving mode

(a) Equivalent circuit in the HPS driving mode; (b) LCC gain curves and working process in the HPS driving mode

As shown in Fig. 3b, the curve (R=∞) is the gain curve of the 3rd order harmonic of $V_{in}(t)$. The operating frequency of the half-bridge is swept down from point A. The voltage across capacitor C_p increases quickly to several thousand volts. At point B, HPS is ignited.

Stage 2: run-up. Once HPS is ignited, the equivalent resistor R_H of HPS becomes very small, and the working point changes from B to C. With the operating frequency being swept down, the fundamental component of $V_{in}(t)$ is dominant. If the operating frequency is much higher than $(2\pi\sqrt{L_sC_s})^{-1}$, the high-order harmonics may be ignored.

The current flowing through the HPS warms it up gradually; meanwhile, the equivalent resistor R_H of HPS increases. If the lamp current is not controlled constantly by the half-bridge, then the operating frequency of the half-bridge drops to the minimum value. At this stage, both the voltage and power of HPS increase.

Stage 3: burn. When the power of HPS is regulated to the rated level, HPS comes to work at its rated power by frequency regulation nearly around point D.

In street lighting applications, dimming is usually required for energy saving. From point D to point E, the gain of the resonant tank drops. Accordingly, the voltage and power of HPS decrease.

2.2 LED driving mode

When the MCU circuit in the driver detects that the LED load is connected, switch S_1 is turned off and S_2 on. The flexible resonant tank changes to LLC

structure, which is accepted as the most popular topology due to its high efficiency in street lighting applications in recent years (Chen *et al*., 2011; Chang *et al*., 2012; Shrivastava and Singh, 2012). Then the driver comes into the LED driving mode. Its equivalent circuit is as illustrated in Fig. 4a. The transformer T transfers isolated energy to LED on the secondary side. The primary leakage inductor L_{LK} of transformer T functions as a resonant inductor L_r together with series inductor L_s. In Fig. 4a, the magnetizing inductor L_m of transformer T, resonant inductor L_r, and resonant capacitor C_r make up the LLC resonant tank, in which capacitor C_s functions as a resonant capacitor C_r. Parameters L_{LK}, L_s, and L_r satisfy

$$L_r=L_s+L_{LK}, \tag{3}$$

$$L_s>>L_{LK}. \tag{4}$$

Note that in mass production, every component has a tolerance. Restricting the tolerance of the component parameter to a smaller range is helpful for the uniformity of the driver. L_r is the key parameter of the resonant tank in the driver. According to Eq. (3) and inequality (4), leakage inductor L_{LK} is much smaller than inductor L_s. Hence, L_s takes more effects in determining parameter L_r. L_{LK} is the leakage inductance of transformer T. Compared with L_s, it is more difficult to narrow the range of tolerance L_{LK}. Consequently, the tolerance of L_r in the flexible resonant can be easily controlled into a small range.

The operating principle of the LLC converter needs to be explained according to its gain curve and *V-I* property. Therefore, the gain of the LLC converter for constant current LED applications should be deduced first.

In Fig. 4a, R_{ac} has the equivalent value of the transformer's secondary load. When the operating frequency is around $(2\pi\sqrt{L_rC_r})^{-1}$, the classical fundamental harmonic analysis (FHA) (Steigerwald, 1988) can be used to analyze the parameters in the circuit. According to FHA, only the fundamental components of voltage and current in the LLC resonant tank are considered.

The voltage on the primary side winding of transformer T is square waveform due to the non-linear rectifiers D_1, D_2 in Fig. 4a. Its sinusoidal fundamental component V_{ac} is applied across the equivalent resistor R_{ac} to analyze the circuit:

$$V_{ac\,\mathrm{rms}}=V_o\frac{2\sqrt{2}}{\pi}N, \tag{5}$$

where $V_{ac\,\mathrm{rms}}$ is the RMS value of V_{ac}.

The DC current I_o flowing through LED is considered as the averaged value of the equivalent current I_{ac} flowing through equivalent resistor R_{ac}. Therefore, I_o and the RMS value $I_{ac\,\mathrm{rms}}$ of the equivalent current I_{ac} satisfy

$$I_o=I_{ac\,\mathrm{rms}}\frac{2\sqrt{2}}{\pi}N. \tag{6}$$

Then Eq. (7) is derived from Eqs. (5) and (6):

$$R_{ac}=8\frac{N^2}{\pi^2}R_L, \tag{7}$$

where N is the turn ratio of transformer T, and R_L is the equivalent resistor of LED.

Since the converter works as a constant current source to drive the LED load, $|I_o/V_{in\_fund}|$ is deduced as the transfer function of the LLC converter:

$$\begin{aligned}G_{LED}(s)&=\frac{I_o}{V_{in\_fund}}=\frac{1}{V_{in\_fund}}I_{ac\,\mathrm{rms}}\frac{2\sqrt{2}}{\pi}N\\&=\frac{2\sqrt{2}N}{\pi}\frac{L_ms}{L_mL_rs^2+R_{ac}(L_r+L_m)s+\frac{R_{ac}}{C_rs}+\frac{L_m}{C_r}},\end{aligned} \tag{8}$$

where V_{in_fund} is the fundamental component of $V_{in}(t)$.

Assume

$$\begin{cases}Q=\dfrac{\sqrt{L_r/C_r}}{R_L},\ f_{r1}=\dfrac{1}{2\pi\sqrt{L_rC_r}},\\ f_{r2}=\dfrac{1}{2\pi\sqrt{(L_r+L_m)C_r}},\ k=\dfrac{f}{f_{r1}},\ m=\dfrac{L_m}{L_r}.\end{cases} \tag{9}$$

Then Eq. (10) is deduced:

$$\left|\frac{I_o}{V_{in\_fund}}\right|=\left|\frac{1}{1+\frac{1}{m}-\frac{1}{mk^2}+Q\frac{\pi^2}{8N^2}\left(k-\frac{1}{k}\right)\mathrm{j}}\right|\cdot\frac{\sqrt{2}\pi}{4NR_L}. \tag{10}$$

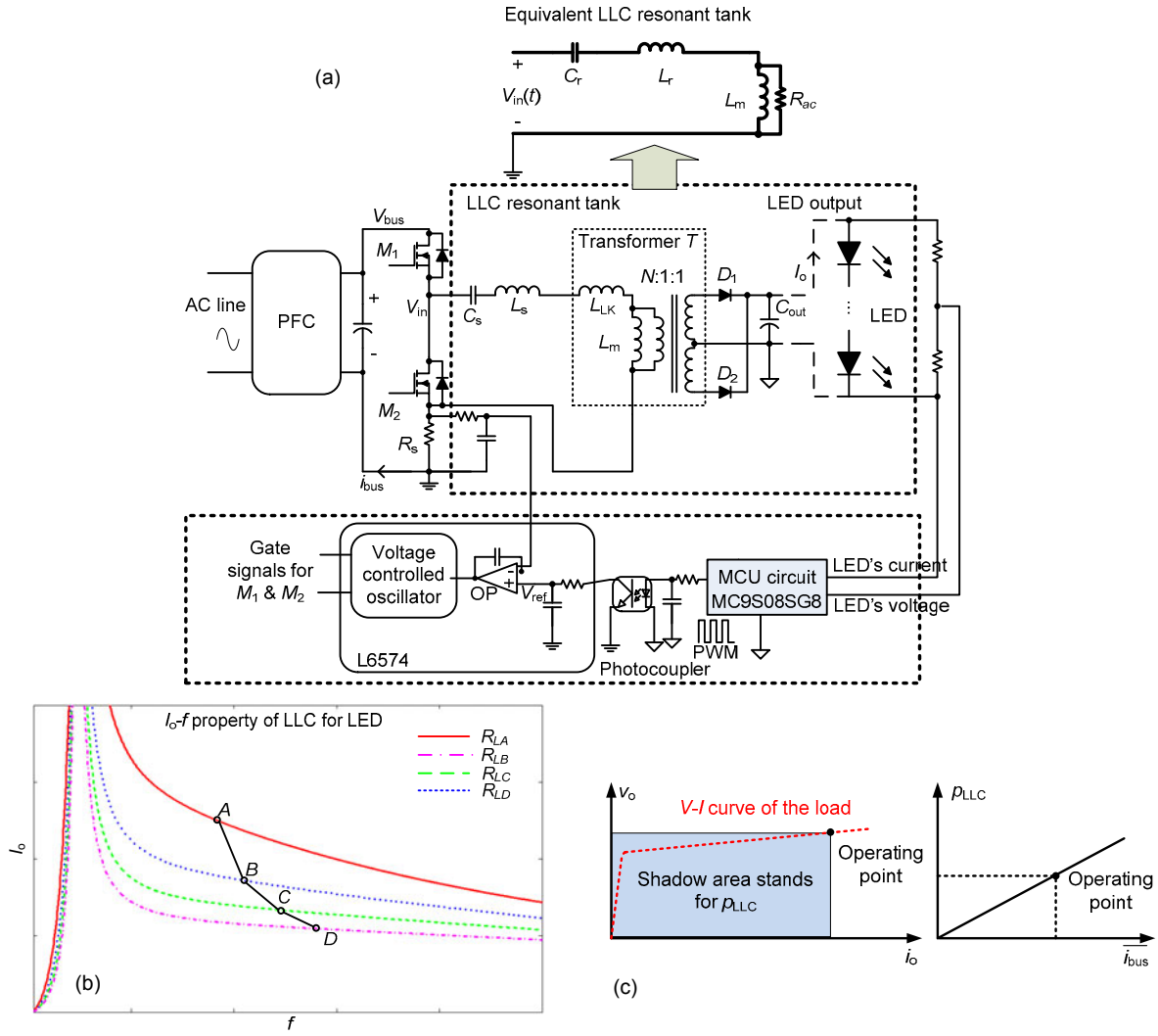

Fig. 4 Driver in the LED driving mode

(a) Equivalent circuit in the LED driving mode; (b) LLC gain curves and the working process of the driver in the LED driving mode; (c) Relationship between output current i_o and average current $\overline{i_{bus}}$ of the LLC converter

Next, the LLC converter's gain curves can be figured (Fig. 4b). Every equivalent resistor has a corresponding gain curve. The vertical axis means the average current flowing through the LED load. Then the frequency can be determined according to the gain curve. The track linking point *A* to point *D* illustrates the dimming process.

The control mechanism is based on the relationship between output current i_o and $\overline{i_{bus}}$ of the LLC converter (Fig. 4c). $\overline{i_{bus}}$ is the average value of input current i_{bus} of the LLC converter. After sampling of output voltage v_o and output current i_o, i_o has a monotonic relationship with power p_{LLC}. Therefore, i_o can be regulated by output power p_{LLC}. Since the input voltage V_{bus} of the LLC converter is constant, the power of LLC converter p_{LLC} is indirectly controlled by $\overline{i_{bus}}$ of the LLC converter. Hence, p_{LLC} is taken as an indirect agent parameter to associate output current i_o and average input current $\overline{i_{bus}}$ of the resonant tank. As a result, i_o can be controlled by regulating $\overline{i_{bus}}$. This working principle is different from the popular LLC control strategy, such as the examples based on L6599 made by ST (STMicroelectronics, 2015b).

From the analysis of the two driving modes above, the proposed driver can compatibly drive both HPS and LED. This multi-functional property can bring convenience for users and manufacturers. Although most circuits are multiplexed in the compatible driver, compared with the traditional LED driver and HPS ballast, its BOM cost still rises and its efficiency slightly decreases. Table 1 lists the advantages and penalties.

Although the BOM cost of the compatible driver is slightly higher, this multi-functional driving solution can save resources for the society, cut down the research and development investments for the producers, and make the implementation simpler for the users. Moreover, the convenience of using the compatible driver makes it a candidate for some applications.

Thus far, the working principle of the flexible resonant tank for compatible driving technology for HPS and LED has been introduced and its transfer functions in different driving mode deduced.

3 Parameter analysis

There is a great difference between the designs of LCC for HPS driving and LLC for LED driving. Conventional design for the resonant tank cares only about one application. In a compatible application, however, the parameters of the resonant tank should support both HPS and LED applications. The performances of the flexible resonant tank in different driving modes need to be analyzed. Moreover, it is necessary to investigate the parameter design principle.

3.1 Specification definition

The key parameters are as defined in Table 2. The values are used for a prototype which is adopted to verify this technology.

3.2 Analysis of parameters for HPS driving mode

The flexible resonant tank changes to LCC structure (Fig. 3a) in the HPS driving mode. The performance of the driver in different stages is introduced in the following.

First, the performance in the burn stage is deduced. The parameters L_s and C_s can be designed in this deduction.

In the burn stage, the current through inductor L_s flows into capacitor C_p and the equivalent resistor R_{Hb} of HPS. For energy efficiency, the major part should better flow into R_{Hb}, so the current through capacitor C_p can be ignored in the burn stage.

Then Eq. (2) is simplified to

$$\left|\frac{V_{\text{HPS\_rated}}}{V_{\text{in\_fund}}}\right| = \left|1\Big/\left(\frac{L_s}{R_{Hb}}\cdot \mathrm{j}2\pi f_{Hw} + \frac{1}{R_{Hb}C_s \mathrm{j}2\pi f_{Hw}} + 1\right)\right|. \tag{11}$$

The capacitor C_s acts mainly as the DC block capacitor. It should satisfy

$$\left|L_s \cdot \mathrm{j}2\pi f_{Hw}\right| >> \left|\frac{1}{C_s \mathrm{j}2\pi f_{Hw}}\right|. \tag{12}$$

L_s is deduced from Eq. (11) and inequality (12) as

$$L_s \approx \frac{1}{2\pi f_{Hw}} R_{Hb}\sqrt{\frac{V_{\text{in\_fund}}^2}{V_{\text{HPS\_burn}}^2} - 1}. \tag{13}$$

Table 1 Comparison between the proposed driver and the traditional driver

Item	Traditional HPS ballast	Compatible driver	Reason
BOM cost	Lower	10%–15% higher	S_1, S_2, T, D_1, D_2, C_{out} are not used in the traditional HPS ballast
Efficiency	Higher	Slightly lower	Power loss of S_1
Universal	No	Yes	
Item	**Traditional LED driver**	**Compatible driver**	**Reason**
BOM cost	Lower	5%–10% higher	S_1, S_2 are not used in the traditional LED driver
Efficiency	Higher	Slightly lower	Power loss of S_2
Tolerance of resonant inductance	Larger	Smaller	L_s is used in the compatible driver, which is helpful for reducing the tolerance of resonant inductance
Universal	No	Yes	

Table 2 Specification of the proposed driver

Specification item	Definition	Parameter	Value
Resonant tank input specification	PFC output	V_{bus}	410 V
	Maximum value of fundamental component input current	$I_{in\_fund\_max}$	10 A
Specification in the HPS driving mode	HPS lamp rated power	P_{HPS_rated}	150 W
	Dimming level of HPS	P_{HPS_dim}	90 W
	Rated lamp voltage at the burn stage	V_{HPS_burn}	95 V
	Lamp voltage at the dimming stage	V_{HPS_dim}	75 V
	Equivalent resistor of HPS at the burn stage	R_{Hb}	60 Ω
	Equivalent resistor of HPS in the dimming condition	R_{Hd}	62.5 Ω
	Maximum ignition voltage	$V_{HPS\_ign\_max}$	3.5 kV
	Minimum ignition voltage	$V_{HPS\_ign\_min}$	2.5 kV
Specification in the LED driving mode	Maximum output current	$I_{o\,max}$	2 A
	Minimum output current	$I_{o\,min}$	1.2 A
	Maximum output voltage	$V_{o\,max}$	48 V
	Equivalent output resistor in the full load condition	$R_{L\,min}$	24 Ω
	Equivalent output resistor in the diming condition	$R_{L\,max}$	33 Ω
Frequency variables	Operating frequency of the resonant tank	f	–
	Operating frequency in the HPS burn stage	f_{Hw}	–
	Operating frequency in the HPS dimming stage	f_{Hd}	–
	The minimum operating frequency of the resonant tank	f_{min}	–
	The maximum operating frequency of the resonant tank	f_{max}	–
	Operating frequency of the resonant tank of the LED driving mode in maximum output current/full load	f_{Lw}	–
	Operating frequency of the resonant tank of the LED driving mode in dimming condition	f_{Ld}	–

For the frequency for HPS, the acoustic resonance free issue should be considered (Lovasoa *et al*., 2012). Dimming level of low power HPS is not advisably lower than 50%–60% for HPS life-time consideration according to Correa *et al*. (2002)

To guarantee that the half-bridge works at ZVS with high efficiency, we have

$$f_{r1} < f_{min}. \tag{14}$$

C_p can be ignored as the current in the resonant tank flows mainly through R_{Hb}. So,

$$C_s = C_r. \tag{15}$$

Substituting Eq. (9) into Eq. (15) leads to

$$C_s > \frac{1}{4\pi^2 f_{min}^2 L_s}. \tag{16}$$

As a result, L_s and C_s can be selected according to inequalities (13) and (16).

Second, the performance in the ignition stage is analyzed. C_p in the resonant tank can be selected in this exploration.

To reduce the sweeping frequency range, the 3rd component of $V_{in}(t)$, instead of the fundamental component, is used to ignite the HPS (Alonso, *et al*., 2003). The equivalent resistor of the lamp is considered infinitely large. Therefore, the transfer function of the LCC resonant tank (Eq. (2)) changes to

$$G_{HPS\_3rd}(s) = \frac{V_{HPS\_ign}}{V_{in\_3rd}} = \frac{1}{9L_r C_p s^2 + \frac{C_p}{C_s} + 1}. \tag{17}$$

Since the ignition voltage should be higher than the minimum ignition threshold in the specification, Eq. (18) should be guaranteed:

$$V_{HPS\_ign} = \frac{V_{in\_3rd}}{|C_p / C_s + 1 - 9L_r C_p (2\pi f)^2|} > V_{HPS\_ign\_min}. \tag{18}$$

During the ignition stage, the higher the voltage

across C_p, the larger the current through it. However, the very high peak current may make the magnetic component L_s saturate. So, the current is also the limitation for L_m:

$$I_{in\_fund} = |V_{HPS\_ign\_max} \cdot C_p \cdot j6\pi f| < I_{in\_fund\_max}. \quad (19)$$

Combining Eqs. (18) and (19) leads to

$$\begin{cases} C_p < \dfrac{I_{in\_fund\_max}}{V_{HPS\_ign\_max} \cdot 6\pi f}, \\ \dfrac{-\dfrac{V_{in\_3rd}}{V_{HPS\_ign\_min}} - 1}{\dfrac{1}{C_s} - 36\pi^2 L_r f^2} < C_p < \dfrac{\dfrac{V_{in\_3rd}}{V_{HPS\_ign\_min}} - 1}{\dfrac{1}{C_s} - 36\pi^2 L_r f^2}. \end{cases} \quad (20)$$

Inequality (20) can be figured to curves (Fig. 5). The value of C_p should be selected within the shadow area crossed by the curves in Fig. 5. The maximum frequency f_{max} should be higher than the frequency f_{Hd} in the dimming condition. Due to the tolerance of the capacitor component, a larger capacitance value of C_p is better for ignition deviation. Here, one value of C_p is selected according to the trade-off principle.

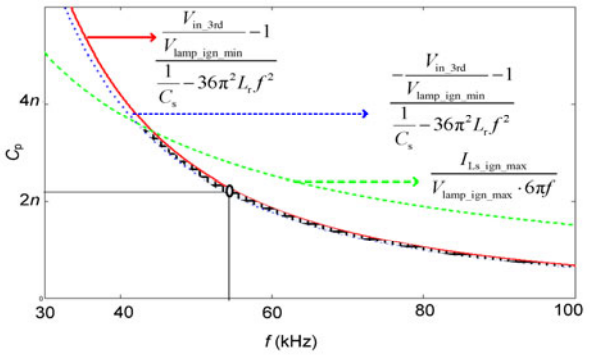

Fig. 5 An example of C_p selection

Third, the performance in the dimming condition is analyzed. The parameters can be evaluated and checked.

Like Eq. (11), in the dimming stage, the transfer function can be expressed as

$$\left|\frac{V_{HPS\_dim}}{V_{in\_fund}}\right| \approx \left|\frac{1}{j2\pi f_{Hd} \cdot L_r / R_{Hd} + 1}\right|. \quad (21)$$

f_{Hd} can be solved as

$$f_{Hd} = \frac{1}{2\pi L_r} R_{Hd} \sqrt{\frac{V_{in\_fund}^2}{V_{HPS\_dim}^2} - 1}. \quad (22)$$

The parameters of the design above should guarantee

$$f_{Hd} < f_{max}. \quad (23)$$

After performance analysis of the driver in different stages in the HPS driving mode, the flexible resonant tank's parameters, including LCC topology, L_s, C_s, C_p, are designed. According to the working principle in Section 2, L_s and C_s are multiplexed as key components in LLC topology.

3.3 Analysis of parameters for LED driving mode

The flexible resonant tank changes to LLC structure (Fig. 4a) in the LED driving mode. The parameters affect the performance of the driver. It can be explained by the output range of the driver and the *V-I* property of the LED load (Fig. 6). Besides parameters L_s and C_s, which are related to the resonant tank as the LCC topology for HPS applications, the other parameters L_m, N of the flexible resonant tank should be designed according to the performance analysis of the driver in the LED driving mode.

As is well known, LED needs to be driven by a constant current for a stable luminous flux density. In Fig. 6, an example is taken that different points *A*, *B*, *C*, *D* on the LED *V-I* property curve represent the different luminous flux densities. In the dimming application, the driver offers the reduced current from point *A* to point *D*. The slope of every point in the coordinates stands for an equivalent resistor of the resonant tank. The curve with points *a*, *b*, *c* is the limitation on the different equivalent resistors, determined by the maximum frequency f_{max}. The curve with points *a*′, *b*′, *c*′ is the limitation on the different equivalent resistors, determined by the minimum frequency f_{min}. The control circuit makes the output CC-CV property of the driver restricted in a square area surrounded by I_{omax}, I_{omin}, V_{omax}, and V_{omin}. In the shadow area surrounded by the curves with points *a*, *b*, *c*, *d*, *e*, the LLC converter works in the continuous mode. In the area below the curve with points *a*, *b*, *c*, the LLC converter comes into the burst mode. Since

in the burst area the ripple of driver's output current is higher and may cause flicker of the load, the driver is not advised to work in this area for a long time. Hence, it is preferred that the operating points are surrounded by the LLC converter's continuous operating area. In the example as shown in Fig. 6, the operating points A, B, C, D are involved in the shadow area with points a, b, c, d, e. This principle is expressed by

$$\begin{cases} V_{\mathrm{o\,max}} \geq V_A, \\ I_{\mathrm{o\,max}} \geq I_D \geq \left|1+\dfrac{1}{m}-\dfrac{1}{mk_{\max}^2}+Q\dfrac{\pi^2}{8N^2}\left(k_{\max}-\dfrac{1}{k_{\max}}\right)\mathrm{j}\right|^{-1} \\ \qquad \cdot\dfrac{\sqrt{2}\pi\cdot V_{\mathrm{in\_fund}}}{4NR_D}, \\ I_{\mathrm{o\,max}} \leq \left|1+\dfrac{1}{m}-\dfrac{1}{mk_{\min}^2}+Q\dfrac{\pi^2}{8N^2}\left(k_{\min}-\dfrac{1}{k_{\min}}\right)\mathrm{j}\right|^{-1} \\ \qquad \cdot\dfrac{\sqrt{2}\pi\cdot V_{\mathrm{in\_fund}}}{4NR_A}, \end{cases} \tag{24}$$

where $k_{\max}$ and $k_{\min}$ are the values of k in Eq. (9) at maximum frequency $f_{\max}$ and minimum frequency $f_{\min}$ respectively, V_A, I_A, V_D, I_D are the voltage and current of operating points A and D, respectively. $R_A=V_A/I_A$, $R_D=V_D/I_D$. The parameter design of the resonant tank should meet the limitation of inequality (24).

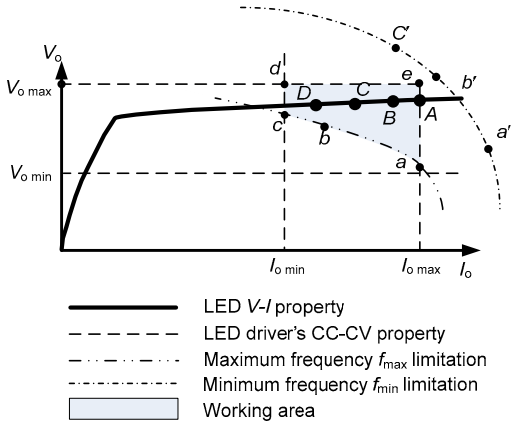

Fig. 6 Output range of the driver and the *V-I* property of the load

Note that FHA is used to analyze the operating frequency around f_{r1}. In the dimming condition, the frequency may be swept higher up to $n{\cdot}f_{\mathrm{r1}}$ (n=3, 5, 7, …) and inequality (24) is not precise any more because the influence of $V_{\mathrm{in}}(t)$'s harmonic components cannot be ignored (Steigerwald, 1988). Some other methods can be used to analyze it (Fang *et al*., 2012). In practical applications, larger margin can be used for inequality (24) to reduce this influence.

The key parameters of the flexible resonant tank in the LED driving mode are related to not only inequality (24), but also the ZVS requirement. A well accepted opinion is that large L_{m} is helpful for reducing the conduction power loss. On the contrary, large L_{m} may affect the ZVS during the dead time of the half-bridge because L_{m} may block the discharge of the equivalent capacitor in parallel with MOSFET. Hence, L_{m} should be chosen as large as possible with

$$L_{\mathrm{m}} \leq \frac{t_{\mathrm{dead}}}{16C_{\mathrm{j}}\cdot f_{\mathrm{r1}}}, \tag{25}$$

$$m \leq \frac{t_{\mathrm{dead}}}{16C_{\mathrm{j}}\cdot f_{\mathrm{r1}}\cdot L_{\mathrm{r}}}, \tag{26}$$

which makes the MOSFET have the ZVS characteristic (C_{j} is MOSFET junction capacitance and t_{dead} is the dead time of the LLC converter) (Lu *et al*., 2006).

Thus far, the parameters L_{m} and N of the flexible resonant tank as LLC topology can be chosen.

After the analysis above, the parameters of the whole flexible resonant tank, related to the performance of the driver in different driving modes, are deduced. As a result, the design principle for the parameters of the flexible resonant tank is provided.

4 Experimental verification

A prototype driver is taken as an example to show the technology. The PFC input voltage is 165–265 V/50 Hz (AC), and the output voltage is 410 V (DC). The specification is listed in Table 2 and the design results of the flexible resonant tank in Table 3.

Table 3 Key parameters of the flexible resonant tank

Parameter	Value	Parameter	Value
Inductor L_{s}	440 μH	Capacitor C_{s}	100 nF
Inductor L_{m}	2.12 mH	Capacitor C_{p}	2.1 nF
Inductor L_{LK}	16 μH	Turn ratio N	3.8

4.1 Experiments in the HPS driving mode

The experiments of the driver are implemented in the HPS driving mode. When the MCU in the driver detects there is no LED connected to the output, it gets into the HPS driving mode. The performances of the driver during the ignition, run-up, and burn stages are verified.

The ignition waveform is provided in Fig. 7a. To observe the maximum voltage of the ignition stage, HPS lamp is not connected in this test. When the operating frequency of the resonant tank is swept down after power on, the output voltage increases quickly. Finally, the ignition voltage stops rising due to the protection of the driver. It can be observed that the high ignition voltage 3.3 kV is up to the required level in Table 2.

The magnified ignition waveforms in Fig. 7b show that the frequency of the output voltage is three times larger than the operating frequency of the half-bridge. The 3rd order harmonic of $V_{in}(t)$ generates the high ignition voltage on capacitor C_p through the resonant tank as analyzed before.

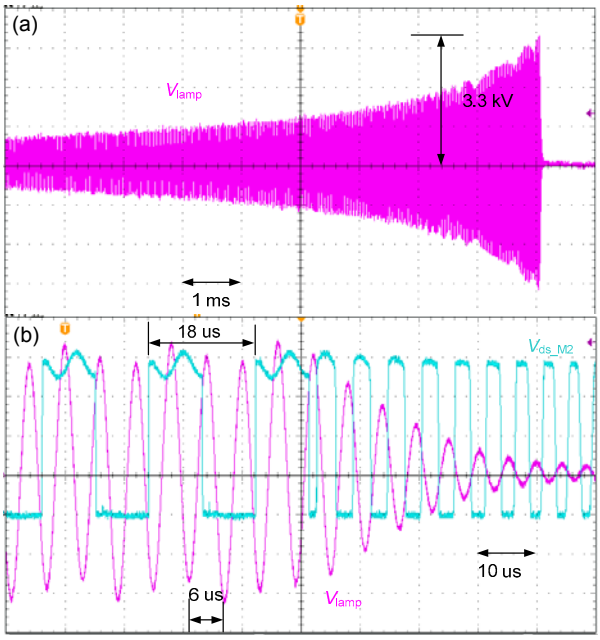

Fig. 7 Ignition waveforms: (a) output voltage of ignition; (b) magnified voltage of ignition

Fig. 8 provides the key waveforms of the driver with the HPS lamp. It illustrates the processes of ignition and run-up stages. After power on, the driver keeps at high frequency to make the resonant tank stable. Then the operating frequency of the driver is swept down towards the minimum value. The output voltage increases quickly and the HPS lamp is ignited. In succession, the driver finishes the ignition stage and comes into the run-up stage. During this stage, the lamp's power increases gradually, its voltage rises, and its current drops until the rated values are reached.

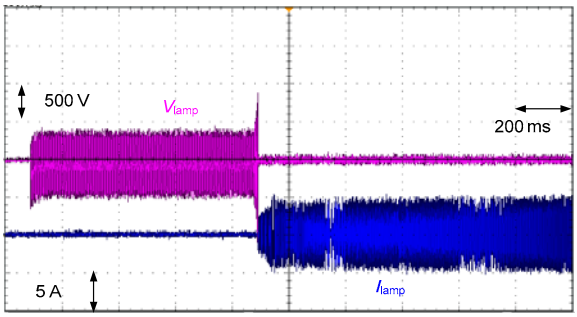

Fig. 8 Key waveforms in the ignition and run-up stages

After the run-up stage and when the power reaches the rated level 150 W specified in Table 2, the driver comes to the burn stage. The waveforms in the burn stage are as illustrated in Fig. 9. The most important characteristic of the resonant tank is the soft-switching, which is illustrated by the waveforms on the low side MOSFET M_2 of the half-bridge.

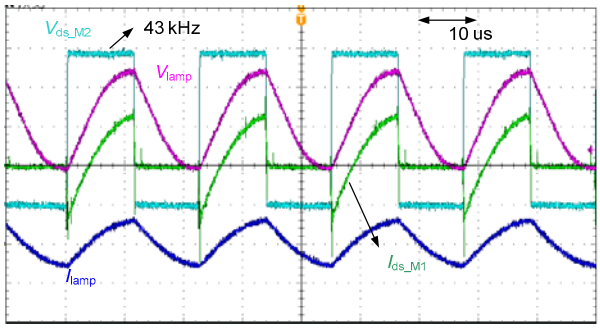

Fig. 9 Key waveforms in the burn stage

In the dimming condition, the operating frequency of the half-bridge increases and the voltage of the lamp decreases (Fig. 3b). The key waveforms are illustrated in Fig. 10.

4.2 Experiments in the LED driving mode

When the LED load is connected to the driver, the driver comes into the LED driving mode under the control of the MCU.

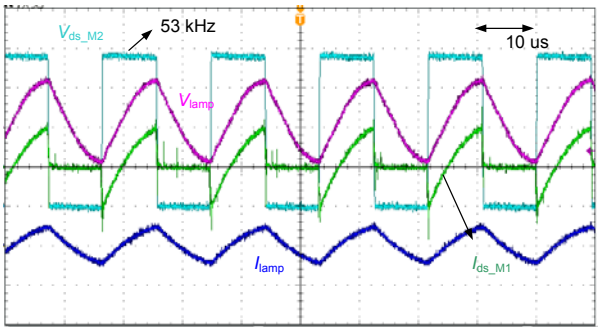

Fig. 10 Dimming waveforms

Both the driver's output range and the LED *V-I* property are tested (Fig. 11). The shadow area is the driver's working area. The results show that the driver can provide proper current to drive the LED load. The parameters of the resonant tank meet the design requirements in Section 3.

The waveforms on the low side MOSFET of the half-bridge, as illustrated in Fig. 12, show that ZVS is realized.

In dimming applications, the operating frequency of the driver increases and the output current drops (Fig. 13). The experimental waveforms of dimming at half of the maximum output current are shown in Fig.13.

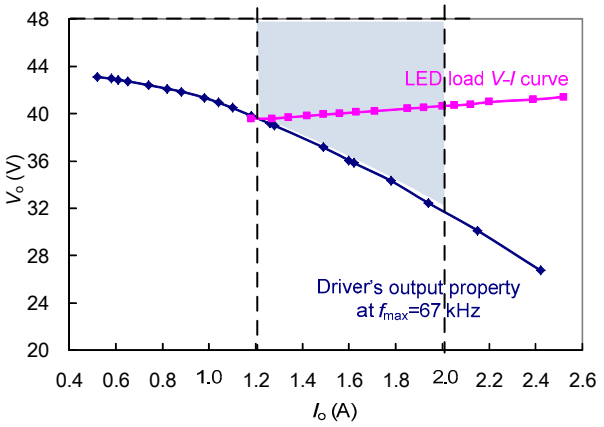

Fig. 11 Test of the driver's output range and LED load's property

4.3 Performance discussion

Efficiency is an important performance of the proposed driver. The test data of the driver in the HPS driving mode and the LED driving mode are provided in Fig. 14. Due to the advantage of ZVS, in the HPS driving mode, the efficiency is approximately 92.7% at 220 V/50 Hz input. In the LED driving mode, the efficiency is about 90% at 220 V/50 Hz input.

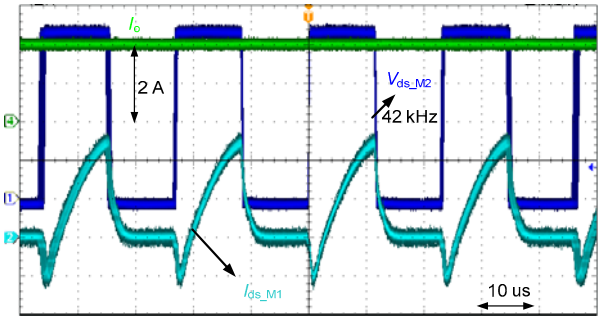

Fig. 12 Working waveforms at maximum output current

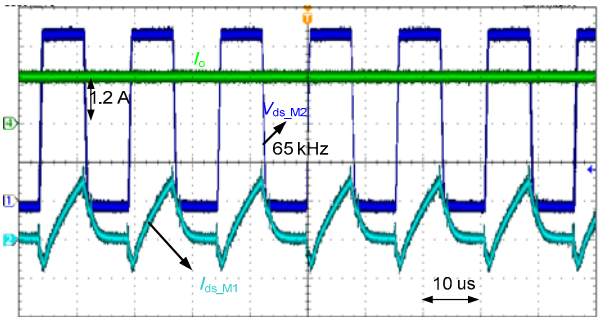

Fig. 13 Working waveforms in the dimming condition

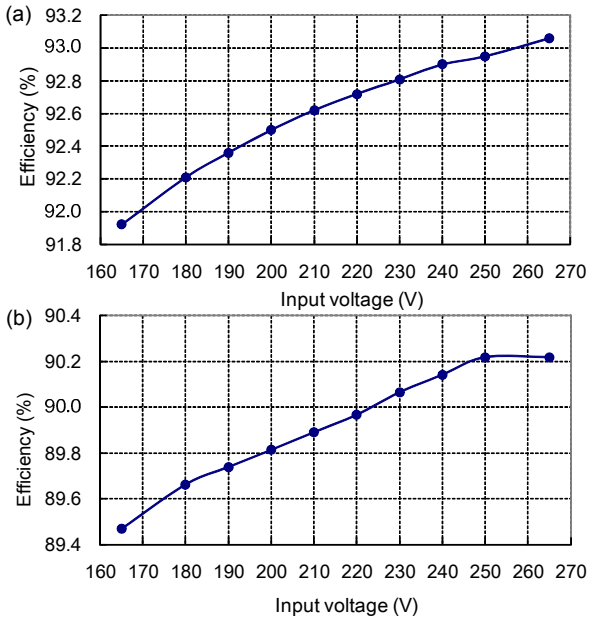

Fig. 14 Efficiency of the compatible driver at different input voltages

(a) Efficiency in the HPS driving mode; (b) Efficiency in the LED driving mode

To make the driver universal for both HPS and LED, some components are added. Hence, the additional power loss is penalized, as introduced in Table 1. Compared with the conventional HPS ballast and LED driver, the efficiencies of the compatible driver in different driving modes are slightly lower.

In addition, the flexible resonant tank should take both HPS and LED into consideration. Hence, it is hard to optimize the parameters of the flexible resonant tank to make the efficiency better than the traditional LCC converter for the HPS ballast or the LLC converter for the LED driver.

Compared with the HPS ballast and LED driver, although the cost and efficiency of the proposed driver have no advantages, the convenience may make it suitable for some applications.

5 Conclusions

A novel HPS and LED compatible driver is proposed. It is a candidate as a multi-functional driver for HPS and LED in large-scale street lighting applications. The traditional HPS ballast usually uses LCC as the driving circuit, and high power LED driver prefers LLC circuit with isolation. Both of them have high efficiency due to the ZVS advantage. The proposed driver combines LLC and LCC into a flexible resonant tank. The flexible resonant tank may change to LLC or LCC based on the light source. It contains the ZVS characteristics and dimmable function of the traditional HPS and LED drivers. When the resonant tank is changed to LLC, another advantage is that the tolerance of the resonant inductor can be well controlled for better consistency in mass production.

Besides the working principle of the proposed compatible driver, the design of the introduced flexible resonant tank is also critical. By considering both of the HPS large gain requirement and LED's isolated constant current output requirement, the performance of this compatible driver is analyzed and the design method for the flexible resonant tank is provided. Compared with the conventional HPS ballast or LED driver, although the BOM cost and efficiency of the proposed driver may have no advantages, it brings convenience for some applications due to compatibility and universality. The experiments on a prototype verify the effectiveness of the proposed driver.

References

Alonso, J.M., Calleja, A.J., Lopez, E., *et al*., 2003. Analysis and design of a HID lamp ballast with sinusoidal waveform superposed with 3rd harmonic. IEEE 34th Annual Power Electronics Specialist Conf., p.971-976.

Azevedo, I.L., Morgan, M.G., Morgan, F., 2009. The transition to solid-state lighting. *Proc. IEEE*, **97**(3):481-510. [doi:10.1109/JPROC.2009.2013058]

Cardesin, J., Alonso, J.M., Lopez-Corominas, E., *et.al*., 2005. Small-signal analysis of a low-cost power control for LCC series-parallel inverters with resonant current mode control for HID lamps. *IEEE Trans. Power Electron.*, **20**(5):1205-1212. [doi:10.1109/TPEL.2005.854066]

Chang, H.S., Lee, B.H., Park, H.N., *et al.*, 2012. Design of dual output LLC resonant converter for a high-power LED lamp. 15th Int. Conf. on Electrical Machines and Systems, p.1-4.

Chen, Y., Wu, X., Qian, Z., *et al*., 2011. Design and optimization of a wide output voltage range LED driver based on LLC resonant topology. IEEE 8th Int. Conf. on Power Electronics - ECCE Asia, p.2831-2837. [doi:10.1109/ICPE.2011.5944780]

Cheng, C.A., Cheng, H.L., Ku, C.W., *et al*., 2014. Design and implementation of a single-stage acoustic-resonance-free HID lamp ballast with PFC. *IEEE Trans. Power Electron.*, **29**(4):1966-1976. [doi:10.1109/TPEL.2013.2266137]

Cheong, C.K., Cheng, K.W.E., Chan, H.L., 2006. Examination of T8-T5 electronic ballast adaptor. 2nd Int. Conf. on Power Electronics Systems and Applications, p.170-172.

Choi, S.C., Jung, D.Y., Kim, J.H., *et al.*, 2013. Control of multi-functional rapid charger for electric vehicle. IEEE Int. Symp. on Industrial Electronics, p.1-6.

Correa, J., Ponce, M., Arau, J., *et al*., 2002. Dimming in metal-halide and HPS lamps operating at HF: effects and modeling. 37th IAS Annual Meeting. Conf. Record of the Industry Applications Conf., p.1467-1474.

Costantini, A., Cavalera, G., Pepino, A., *et al*., 2011. A CMOS low-power SoC for HID and LED lamps ballast. 7th Conf. on Ph.D. Research in Microelectronics and Electronics, p.109-112.

Fang, X., Hu, H., Shen, Z.J., *et al*., 2012. Operation mode analysis and peak gain approximation of the LLC resonant converter. *IEEE Trans. Power Electron.*, **27**(4):1985-1995. [doi:10.1109/TPEL.2011.2168545]

Huang, C.M., Liang, T.J., Lin, R.L., *et al*., 2007. A novel constant power control circuit for HID electronic ballast. *IEEE Trans. Power Electron.*, **22**(5):1573-1582. [doi:10.1109/TPEL.2007.904159]

IEC, 2006. IEC 61347-2-13:2006. Lamp Control Gear. Part 2-13: Particular Requirements for d.c. or a.c. Supplied Electronic Control Gear for LED Modules.

IEC, 2011. IEC 60662:2011. High-Pressure Sodium Vapour Lamps-Performance Specifications.

Kirsten, A.L., Dalla Costa, M.A., Rech, C., *et al*., 2013. Digital control strategy for HID lamp electronic ballasts. *IEEE Trans. Ind. Electron.*, **60**(2):608-618. [doi:10.1109/TIE.

2012.2205363]

Ko, S.H., Lim, S.H., Lee, S.R., *et al.*, 2007. Operational characteristics of fault current limiting reactor combined with multi-functional invertor. IEEE 7th Int. Conf. on Power Electronics and Drive Systems, p.1719-1723.

Lee, L.M., Hui, S.Y.R., 2009. Automatic lamp detection and operation for warm-start tubular fluorescent lamps. *IEEE Trans. Power Electron.*, **24**(12):2933-2941. [doi:10.1109/TPEL.2009.2023363]

Lovasoa, R.F., Zely, R.A., Dorin, L.D., *et al*., 2012. Energetic aspects of the HID ballast used in the outdoor lighting. Int. Conf. and Exposition on Electrical and Power Engineering, p.340-346.

Lu, B., Liu, W., Liang, Y., *et al*., 2006. Optimal design methodology for LLC resonant converter. 21st Annual IEEE Applied Power Electronics Conf. and Exposition, p.533-538.

Moksoon, J., Byounglo, L., Chongyeun, P., 2008. An optimal LCC design method for dimmable electronic ballasts of the HID lamp. IEEE Industry Applications Society Annual Meeting, p.1-8.

Mu, H., Geng, L., Liu, J., 2011. A high precision constant current source applied in LED driver. IEEE Symp. on Photonics and Optoelectronics, p.1-4.

Nan, C., Chung, H.S.H., 2011. A driving technology for retrofit LED lamp for fluorescent lighting fixtures with electronic ballasts. *IEEE Trans. Power Electron.*, **26**(2):588-601. [doi:10.1109/TPEL.2010.2066579]

Rodrigues, C., Guedes, L., Rodrigues, M., *et al.*, 2009. Single electronic ballast for HPS and HPMV lamp testing. IEEE Power Electronics Conf., p.586-592.

Schnell, R.W., Zane, R.A., Azcondo, F.J., 2013. Size reduction in low-frequency square-wave ballasts for high-intensity discharge lamps using soft-saturation magnetic material and digital control techniques. *IEEE Trans. Power Electron.*, **28**(2):1036-1046. [doi:10.1109/TPEL.2012.2202129]

Shrivastava, A., Singh, B., 2012. LLC series resonant converter based LED lamp driver with ZVS. IEEE 5th Power India Conf., p.1-5.

Steigerwald, R.L., 1988. A comparison of half-bridge resonant converter topologies. *IEEE Trans. Power Electron.*, **3**(2):174-182. [doi:10.1109/63.4347]

STMicroelectronics, 2015a. AN2708: 2X36 W Digital Dimmable Ballast with L6574 and ST7FDALI. Available from http://www.st.com/web/en/resource/technical/document/application_note/CD00184169.pdf [Accessed on Feb. 6, 2015].

STMicroelectronics, 2015b. AN3106: 48 V-130 W High-Efficiency Converter with PFC for LED Street Lighting Applications. Available from http://www.st.com/web/en/resource/technical/document/application_note/CD00256070.pdf [Accessed on Feb. 6, 2015].

Tan, S.C., 2010. General level driving approach for improving electrical-to-optical energy-conversion efficiency of fast-response saturable lighting devices. *IEEE Trans. Ind. Electron.*, **57**(4):1342-1353. [doi:10.1109/TIE.2009.2029515]

Tomoroga, M., Jivet, I., Nicoara, D., 2012. Intelligent telemanagement of street lighting equipped with HID lamps. 10th Int. Symp. on Electronics and Telecommunications, p.7-10.

Visconti, P., Zizzari, G., Romanello, D., *et al*., 2011. Electronic board for driving of HID and LED lamps with auxiliary power supply from solar panel and presence detector. 10th Int. Conf. on Environment and Electrical Engineering, p.1-4.

Wang, H., Liu, Z., Dong, J., 2011. High-power LED constant-current driver circuit design and efficiency analysis. Proc. IEEE Cross Strait Quad-Regional Radio Science and Wireless Technology Conf., p.705-710. [doi:10.1109/CSQRWC.2011.6037049]

Wang, Y., Zhang, X., Xu, D., *et al.*, 2011. Design optimisation of the LCsCp resonant inverter to drive 1 kW high-pressure sodium lamps. *IET Power Electron.*, **4**(4):374-383. [doi:10.1049/iet-pel.2010.0127]

Wei, Y., Hui, S.Y.R., Chung, H.S.H., 2009. Energy saving of large-scale high-intensity-discharge lamp lighting networks using a central reactive power control system. *IEEE Trans. Ind. Electron.*, **56**(8):3069-3078. [doi:10.1109/TIE.2009.2022089]

Wu, H., Ji, S., Lee, F.C., *et al.*, 2011. Multi-channel constant current (MC 3) LLC resonant LED driver. IEEE Energy Conversion Congress and Exposition, p.2568-2575.

Zhao, B., Song, Q., Liu, W., *et al*., 2013. Next-generation multi-functional modular intelligent UPS system for smart grid. *IEEE Trans. Ind. Electron.*, **60**(9):3602-3618. [doi:10.1109/TIE.2012.2205356]

Zhu, J., Zhuo, F., Wang, Z., 2009. Design of a digital controller for high frequency HID lamp ballast. IEEE 6th Int. Power Electronics and Motion Control Conf., p.2516-2520.

Zotos, N., Stergiopoulos, C., Anastasopoulos, K., *et al.*, 2012. Case study of a dimmable outdoor lighting system with intelligent management and remote control. IEEE Int. Conf. on Telecommunications and Multimedia, p.43-48.